Optimizing the Cation Binding Pocket in Nickel Phenoxyimine Catalysts Improves Ethylene Polymerization Efficiency

Lorenzo C. Ruiz De Castilla,[†] Tuhin Ganguly,[†] Babak Tahmouresilerd, Croix J. Laconsay, Judy I. Wu, Loi H. Do*
Department of Chemistry, University of Houston, Houston, Texas 77004, United States

[†]These authors contributed equally.

ABSTRACT: Cation tuning is a simple yet powerful strategy to modulate the reactivity of polymerization catalysts but the design rules to achieve maximum cation effects are not well understood. In the present work, it was demonstrated that inserting a methylene spacer between a nickel phenoxyimine complex and an M-polyethylene glycol (PEG) (where M = Li^+, Na^+, K^+, or Cs^+) unit led up to >70-fold increase in ethylene polymerization activity and 6-fold higher polymer molecular weight relative to that of the first-generation catalysts. It is hypothesized that these effects are due to the exclusive formation of 1:1 over 2:1 nickel:alkali species and closer proximity of the M-PEG moiety to the nickel center. These results suggest that the successful creation of cation-responsive catalysts requires an understanding of the cation binding stoichiometry as well as the structural and electronic changes associated with its host-guest interactions.

INTRODUCTION

Polyolefins are produced on enormous scales each year using coordination-insertion polymerization.[1-3] Industrial processes typically rely on early transition metal catalysts that are extremely fast and thermally-robust. However, there is growing interest in studying late transition metal catalysts (e.g., Ni and Pd)[4-8] for olefin polymerization because they can chain walk to give branched polymers starting from only ethylene and are compatible with certain polar monomers. Due to the significantly lower cost of nickel relative to palladium, the development of high-performance Ni catalysts is attractive for practical reasons.[9,10] A few notable families of nickel catalysts include those supported by diimine,[11,12] phenoxyimine,[13,14] phenoxyphosphine,[10] α-ketoimine,[15,16] and pyridylimine[17,18] ligands. Although some of these polymerization catalysts exhibit unique attributes, such as the ability to generate ultra-high molecular weight polymers with branches[19] or incorporate monomers containing protic groups[20], none have yet been commercialized to the best of our knowledge.

To endow polymerization catalysts with switchability, researchers have utilized ligand platforms that respond to external stimuli, such as light, redox agents, or boranes.[21-23] The use of inorganic cations to bolster olefin polymerization was first demonstrated by DuPont and Brookhart with a nickel alkoxyphosphine catalyst system (**Cat1**) (Chart 1A).[24] Our laboratory expanded on this concept by showing that a conventional nickel phenoxyimine complex could be made cation-responsive by installing a short polyethylene glycol (PEG) chain *ortho* to the phenolate ring (**Cat2**).[25,26] We observed that the catalyst activity and polymer products produced by **Cat2** varied dramatically depending on the alkali ion used (e.g., Li^+, Na^+, or K^+). Additionally, by exploiting the cation exchange equilibrium between a nickel catalyst (e.g., **Cat3**) and external cations in solution, dynamic polymerization was achieved in which chain growth in non-living reactions were controlled.[27] Similar design strategies were used by others to expand the repertoire of cation-responsive olefin polymerization catalysts,[28] including a palladium aryloxy *N*-heterocyclic carbene (**Cat4**),[29] dinickel bis(phosphine)BINOL (**Cat5**) complexes,[30] and others.[31-33]

Chart 1. Examples of cation-responsive olefin polymerization catalysts reported in the literature (A) and optimization of the cation binding pocket in this work (B).

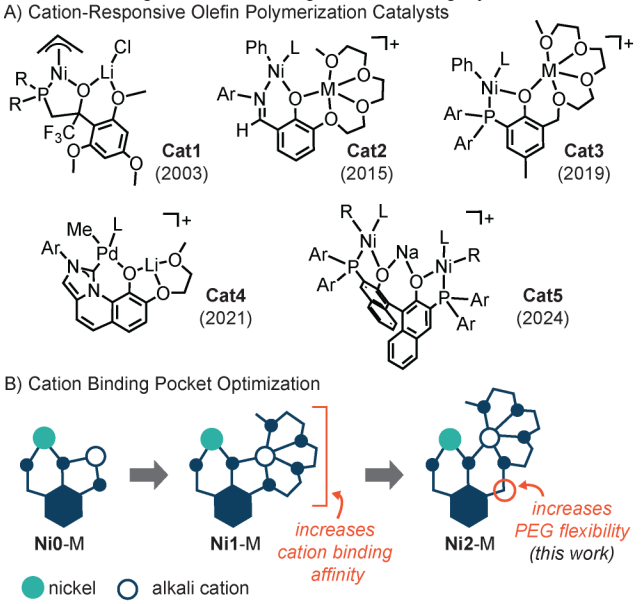

Among the Ni catalysts, nickel phenoxyphosphine complexes (e.g., **Cat3** and **Cat5**) are the most versatile due to their

faster rates and better functional group tolerance but synthesizing and handling them can be challenging.[10,34-37] In contrast, although **Cat2** is more synthetically accessible than **Cat3**/**Cat5**, it generally exhibits inferior performance. For example, catalysts derived from nickel phenoxyimine have *not* been reported to copolymerize ethylene with polar vinyl monomers[38,39] whereas nickel phenoxyphosphines can copolymerize ethylene with a variety of functional olefins (e.g., alkyl acrylate and acrylamide).[30,34-36] Because nickel phenoxyimine complexes are relatively straightforward to synthesize, efforts to unlock new reactivity using these platforms could make them more attractive as industrially-viable catalysts.

To enhance the performance of the nickel phenoxyimine systems, we rely on an iterative design process (Chart 1B). We demonstrated previously that the PEG chain in our first-generation catalyst **Ni1** (Scheme 1) is essential for stabilizing cation adducts, since the parent **Ni0** with only an ortho methoxy group on the phenolate did not interact with M^+.[25] Herein, we show that inserting a methylene spacer between the phenolate ring and PEG group greatly increases the ethylene polymerization activity and polymer molecular weight of the corresponding **Ni2**-M species relative to that of **Ni1**-M (where M = Li^+, Na^+, K^+, or Cs^+). These results demonstrate that seemingly minor ligand modifications could lead to dramatic changes to the catalyst properties,[40] which is an important lesson to carry forward in future catalyst design endeavors.

RESULTS AND DISCUSSION

Catalyst Design and Synthesis. Our first-generation catalyst **Cat2** showed cation responsive reactivity but has a propensity to form both 1:1 and 2:1 nickel:alkali species in solution,[25,26] which would prevent single-site polymerization. To favor the exclusive formation of 1:1 nickel:alkali species, we drew inspiration from the design of **Cat3** (Chart 1A),[41,42] which has a methylene group linking the phenolate and PEG. This structural feature was believed to be key to controlling the cation binding stoichiometry.

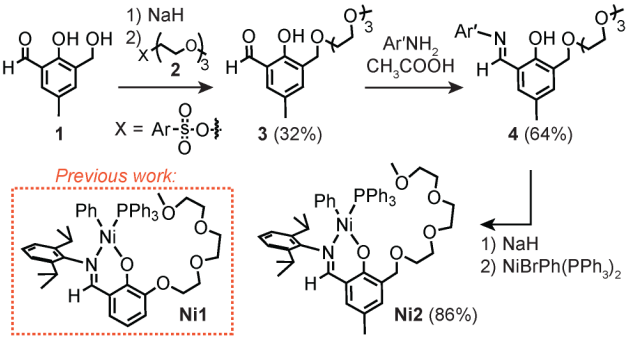

Scheme 1. Synthetic route for the preparation of complex **Ni2**. Ar = 2, 4, 6- tris(isopropyl)phenyl, Ar′ = 2,6-diisopropylaniline.

Based on the above, we prepared a second-generation nickel phenoxyimine complex bearing a methylene extended PEG chain (**Ni2**, Scheme 1). Due to the commercial availability of one of the starting materials, this complex also bears a methyl group at the para position of the phenolate ring but this modification is unlikely to have significant effects on the catalyst's properties. The synthesis involves first monooxidation of 2,6-bis(hydroxymethyl)-*p*-cresol using MnO_2 to provide **1** in 73% yield, followed by treatment with sodium hydride, and alkylation with **2** to afford compound **3** in 32% yield. Imine condensation was performed by combining **3** with 2,6-diisopropylaniline and acetic acid, giving the desired ligand **4** as a yellow oil after purification by silica gel column chromatography (64% yield). Finally, deprotonation of **4** with sodium hydride and reaction with $NiBrPh(PPh_3)_2$ furnished **Ni2** as a yellow solid after recrystallization (86% yield). This complex was fully characterized, including by NMR and IR spectroscopy and mass spectrometry. X-ray crystallographic analysis of single crystals of **Ni2** grown from THF/pentane shows that the nickel center has the expected square planar geometry (Figure S35) with the phenoxyimine, phenyl, and triphenylphosphine ligands occupying its coordination sphere.

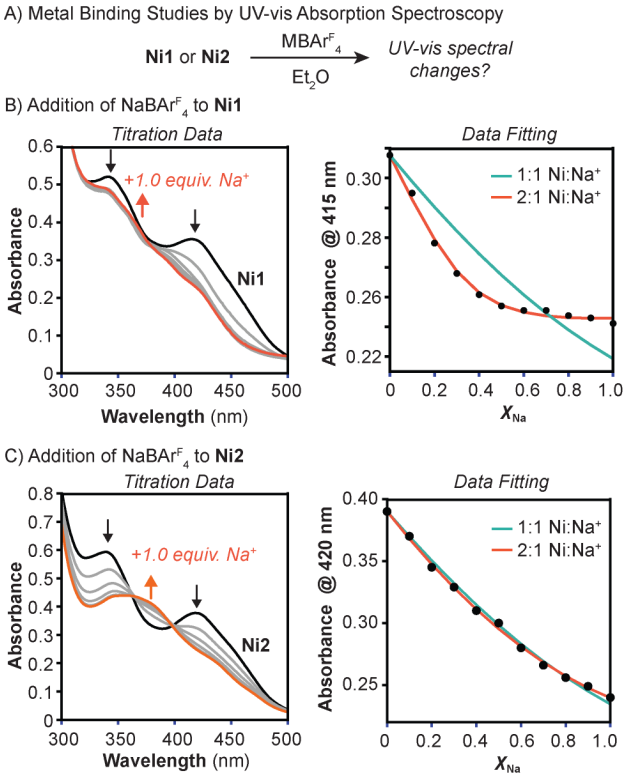

Figure 1. Studying the binding of alkali ions to the nickel complexes by UV-vis absorption spectroscopy in Et_2O (A). Representative examples showing the addition of $NaBAr^F_4$ to **Ni1** (B) and **Ni2** (C). The full titration plot is shown on the left and the single wavelength data fits are shown on the right. The data were fit to either a 1:1 (turquoise line) or 2:1 (red orange line) nickel:alkali equilibria using the program BindFit v5.0. X_{Na} = the ratio of sodium/nickel.

Metal Binding Studies by UV-vis Absorption Spectroscopy. The nickel:alkali binding stoichiometries of the newly synthesized **Ni2** were determined using UV-vis absorption spectroscopy (Figures 1).[25,42] To perform these experiments, the nickel complex was dissolved in Et_2O in a quartz cuvette and aliquots containing 0.1 equiv. of $MBAr^F_4$ (where $BAr^F_4{}^-$ = tetrakis(3,5-bis(trifluoromethyl)phenyl)borate anion) relative to Ni were added (Figure S1). Although our polymerization reactions are carried out in toluene/Et_2O (96:4) (vide infra), the use of 100% Et_2O was necessary here to ensure that the $MBAr^F_4$ salts are completely dissolved in their concentrated stock solutions. It is possible that the binding affinities are different in toluene/Et_2O compared to in Et_2O but the Ni:M^+ stoichiometries are expected to be the same in both solvent mixtures. Under our titration conditions, the introduction of M^+ to **Ni2** resulted in

gradual spectral changes with the appearance of distinct isosbestic points. For example, the addition of $NaBAr^F_4$ to **Ni2** led to absorption decreases at 340 and 420 nm concomitant with absorption increases at 370 nm (Figure 1C). Adding more than 1.0 equiv. of $NaBAr^F_4$ relative to Ni did not result in further changes. Next, the titration data were subjected to BindFit analysis to determine the Ni:M^+ stoichiometry.[43,44] Two different binding models were compared, based on the following equilibria:

$$Ni + M^+ \rightleftharpoons NiM \quad K_a = [NiM]/[Ni][M^+] \quad \text{(Eq. 1)}$$

$$NiM + Ni \rightleftharpoons Ni_2M \quad K_b = [Ni_2M]/[NiM][Ni] \quad \text{(Eq. 2)}$$

The 1:1 model includes only the formation of NiM species (Eq. 1 only) whereas the 2:1 model includes the formation of both NiM and Ni_2M species (Eqs. 1 and 2). Although the titration data for **Ni2**+M^+ at 420 nm could be fit satisfactorily to either the 1:1 or 2:1 models (Figures 1C and S2), the former is most likely due to the presence of isosbestic points and absorbance changes beyond the addition of 0.5 equiv. of M^+ (Scheme 2B). Based on the association constants (K_a) derived from the 1:1 fits, the affinity of **Ni2** for the alkali ions follow the order $Na^+ > K^+ > Cs^+ \sim Li^+$ (K_a ranges from ~2000 to 33000, Table S1).

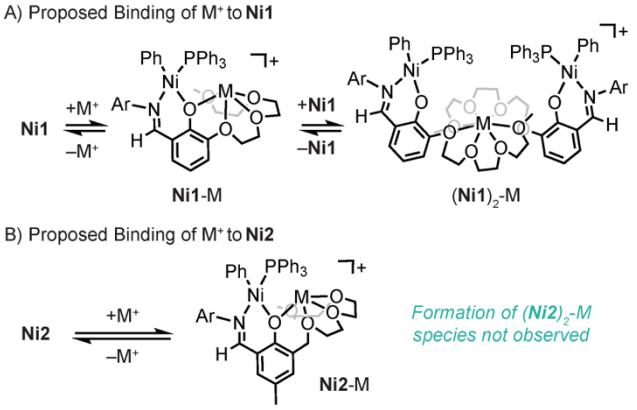

Scheme 2. Proposed binding models for the addition of M^+ to the nickel complexes **Ni1** (A) and **Ni2** (B). The (**Ni1**)$_2$-M structure is putative.

For comparison, we carried out similar titration studies using **Ni1** in Et_2O. Our results showed that combining **Ni1** with $MBAr^F_4$ led to clear spectral changes, indicating that the cations interact with the nickel complex. However, unlike in the experiments above using **Ni2**, no distinct isosbestic points were observed (Figures 1B and S3). The absorbance changed most significantly with up to ~0.5 equiv. of Na^+ addition relative to Ni and then the changes were more gradual, suggesting that more than one new species had formed. BindFit analysis of the absorption data at 415 nm shows that the 2:1 model is a better fit than the 1:1 model (Figure S4). Because some of the calculated association constants for the two chemical equilibria (K_a and K_b) had large standard deviations (>15%), there is low confidence in the numerical values (Table S2). However, these results are consistent with our reported work showing that both **Ni1**-M and (**Ni1**)$_2$-M species were generated upon the addition of M^+ to **Ni1** (Scheme 2A).[25]

Metal Binding Studies by NMR Spectroscopy. To probe the nature of M^+ binding to the nickel complexes further, we conducted studies using NMR spectroscopy. Samples containing either **Ni1** or **Ni2** were stirred in the presence of 0.5 or 1.5 equiv. of M^+ in Et_2O for 30 min and then evaporated to dryness. The resulting products were then redissolved in toluene-d_8/Et_2O (2:1) for NMR spectroscopic analysis (Figure 2A). This solvent mixture was used to mimic the polymerization conditions as closely as possible while enabling complete dissolution of the $MBAr^F_4$ salts.

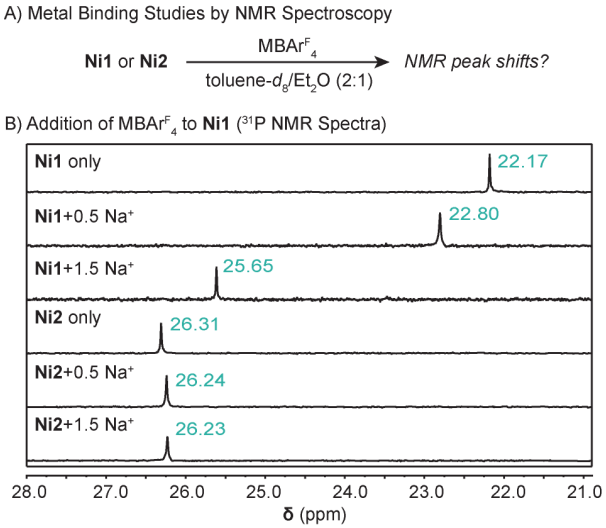

C) ^{31}P NMR Chemical Shift Comparison

	+0.5 equiv. M^+		+1.5 equiv. M^+		
	δ (ppm)	Δδ	δ (ppm)	Δδ	
Ni1	22.17	-	22.17	-	
Ni1+Li^+	22.49	-0.32	23.27	-1.10	*maximum chemical shifts relative to **Ni1** ≤3.48 ppm*
Ni1+Na^+	22.80	-0.63	25.65	-3.48	
Ni1+K^+	22.14	0.03	25.61	-3.44	
Ni1+Cs^+	22.39	-0.22	24.93	-2.76	
Ni2	26.31		26.31		
Ni2+Li^+	26.17	0.14	25.91	0.4	*maximum chemical shifts relative to **Ni2** ≤0.37 ppm*
Ni2+Na^+	26.24	0.07	26.23	0.08	
Ni2+K^+	26.43	-0.12	26.09	0.22	
Ni2+Cs^+	26.28	0.03	25.94	0.37	

Figure 2. A) Studying the binding of alkali ions to the nickel complexes by NMR spectroscopy in toluene-d_8/Et_2O (2:1). B) ^{31}P NMR spectra showing the addition of $NaBAr^F_4$ to **Ni1** and **Ni2**. C) A comparison of the ^{31}P chemical shifts of the nickel complexes upon addition of 0.5 or 1.5 equiv. of M^+ relative to Ni.

Our results provided additional insights into the nickel and nickel-alkali species. First, the ^{31}P NMR peaks corresponding to the phosphine ligands in **Ni1** (22.17 ppm, Figure 2B) and **Ni2** (26.31 ppm, Figure 2C) have similar chemical shifts, suggesting that the nickel complexes are electronically similar despite being ligated by phenolate donors with slightly different substituents. Second, the ^{31}P chemical shifts appear to be more sensitive to the presence of M^+ in **Ni1** than **Ni2**. We observed that the addition of 1.5 equiv. of M^+ to **Ni1** gave a maximum Δδ ($\delta_{Ni} - \delta_{Ni+M}$) of 3.48 ppm, compared to 0.37 ppm for **Ni2** (Figure 2C). Given that the ^{31}P NMR chemical shift scale typically range from -250 to 250 ppm,[45,46] a <0.4 ppm shift is likely a negligible change. Although a possible interpretation of these results is that M^+ does not bind to the phenolate oxygen in **Ni2**, crystallographic studies of a related nickel-P,O complex, which has an identical cation binding pocket, showed phenolate coordination

to Li^+, Na^+, K^+, and Cs^+ in a 1:1 alkali-to-nickel ratio.[27,42] We hypothesize that the insensitivity of the ^{31}P NMR chemical shift to M^+ binding in **Ni2** is due to the presence of the methylene group between the phenolate and PEG, which minimizes the electronic effects of M^+ experienced by the nickel center. More detailed investigations, however, are needed to fully understand these results. Third, the different chemical shifts of **Ni1** samples containing different amounts of M^+ suggest that more than one nickel:alkali species may be accessible (Figures S5-S6). For example, when **Ni1** was treated with 0.5 and 1.0 equiv. of Na^+, the ^{31}P peaks appeared at 22.80 and 25.65 ppm, respectively (Figure 2B). Based on the 2:1 model proposed in Scheme 2, we have assigned these peaks to the presence of (**Ni1**)$_2$-Na when 0.5 equiv. of Na^+ was added and **Ni1**-Na when 1.0 equiv. of Na^+ was added. Similar results were obtained when **Ni1** was combined with Li^+, K^+, or Cs^+ (Figures S5-S6).

Lastly, the introduction of alkali salts to **Ni1** afforded a phosphorus-containing product that features a resonance at 23.4 ppm (Figure S6). Although the identity of this species is unclear, it is likely not coordinated to nickel due to the sharpness of its ^{31}P NMR signal and is not free PPh_3 (-4.9 ppm) or $OPPh_3$ (24.4 ppm) based on the chemical shifts of the authentic compounds. No such phosphorus-containing byproducts were observed in samples containing **Ni2** and M^+.

Taken together, our metal binding studies revealed that **Ni2** interacts with alkali ions in a more predictable manner than **Ni1** (i.e., the former likely produces 1:1 nickel:alkali species and do not generate unknown phosphorus-containing byproducts), which was expected to to have significant effects on its catalytic performance.

DFT Calculations of Nickel-Alkali Structures. It is clear from the above that additional structural information is needed to fully understand the effects of M^+ on **Ni1** and **Ni2**. Unfortunately, despite our best efforts, we were unable to grow single crystals of the nickel-alkali species for X-ray diffraction analysis. As an alternative, we turned to density functional theory calculations to gain structural insights.[47] Utilizing the ωB97X-D functional and def2-SVP basis set, we calculated energy-minimized structures for the **Ni1**-M and **Ni2**-M series in the gas phase. Because the structure of **Ni1**-Na was crystallographically characterized in our previous work,[25] it was used as a starting point for the calculations; however, we varied the alkali ion and phenoxyimine ligand as appropriate and then allowed full geometry optimization to proceed. In general, the computed nickel-alkali conformers exhibit pseudo square planar nickel centers ligated by the *N*,*O*-donor of the supporting ligand, triphenylphosphine, and phenyl group. The alkali ions reside within the binding pocket defined by the PEG chain and phenolate donor. The four oxygen atoms in PEG are ligated to the alkali ions, except in **Ni2**-Li and **Ni2**-K, in which only three oxygen atoms in PEG are ligated. A key difference between the **Ni1**-M vs. **Ni2**-M structures is that the presence of a methylene spacer in the latter enables the M-PEG unit to be positioned closer to the nickel center (Figure 3A). For example, the Ni–M atomic distance are shortened by 0.18, 0.02, 0.66, and 0.37 Å in **Ni2**–Li, **Ni2**–Na, **Ni2**–K, and **Ni2**–Cs relative to that in **Ni1**–Li, **Ni1**–Na, **Ni1**–K, and **Ni1**–Cs, respectively (Figure 3B). The closer proximity of the M-PEG moiety to Ni may also restrict the rotational freedom of the ancillary 2,6-diisopropylphenyl group and potentially lead to better axial shielding of the nickel center.

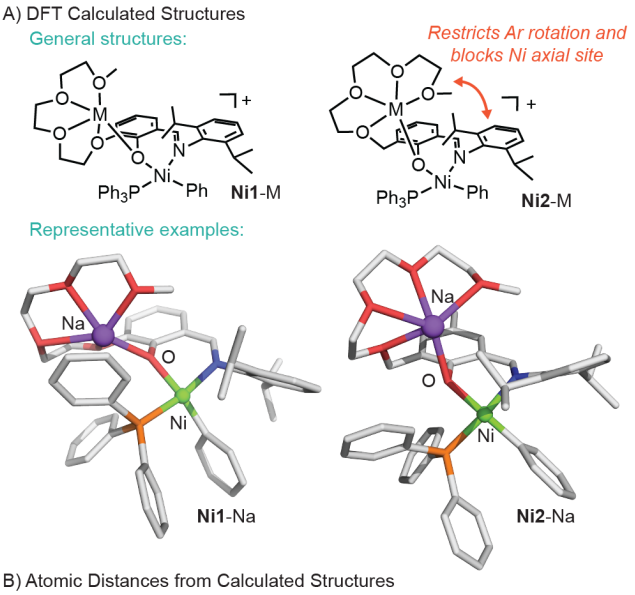

B) Atomic Distances from Calculated Structures

	M–O	Ni–O	Ni–M
Ni1-Li	1.881	2.028	3.725
Ni1-Na	2.198	2.029	4.029
Ni1-K	2.518	1.981	4.398
Ni1-Cs	2.743	1.979	4.446

	M–O	Ni–O	Ni–M
Ni2-Li	1.872	2.000	3.543
Ni2-Na	2.333	1.971	4.013
Ni2-K	2.619	1.958	3.743
Ni2-Cs	2.846	1.952	4.074

Figure 3. Comparison of the DFT (ωB97X-D/def2-SVP) calculated structures between **Ni1**-M vs. **Ni2**-M showing differences in the positions of their M-PEG units relative to the nickel center (A). The calculated structures of **Ni1**-Na and **Ni2**-Na are shown as representative examples (atom colors: green = nickel, purple = sodium, orange = phosphorus, red = oxygen, blue = nitrogen, gray = carbon; hydrogen atoms were omitted for clarity). Select atomic distances (Å) for the various nickel-alkali complexes are provided in part B.

Table 1. Ethylene Polymerization Data[a]

Entry	Cat.	M^+	Act. (kg/mol Ni·h)	M_n[b] (kg/mol)	$Đ$[b]	Branch.[c] (/1000 C)
1	**Ni1**	none	2	1.8	1.1	34
2	**Ni1**	Li^+	4.6	3.2	1.3	67
3	**Ni1**	Na^+	21.3	9.6	2.0	102
4	**Ni1**	K^+	16.7	3.1	3.6	101
5	**Ni1**	Cs^+	13.6	7.7	1.8	89
6	**Ni2**	none	2	2.0	1.1	22
7	**Ni2**	Li^+	332	18	2.0	67
8	**Ni2**	Na^+	112	13	1.4	79
9	**Ni2**	K^+	70	14	1.6	70
10	**Ni2**	Cs^+	21	11	2.0	39

[a]Reaction conditions: Ni catalyst (24.0 μmol), $MBAr^F_4$ (24 μmol, if any), $Ni(COD)_2$ (2.0 equiv.), 50 mL toluene:Et_2O (96:4), 200 psi ethylene (constant feed), 25 °C, 1 h. The temperature was maintained within ±5 °C by external cooling using compressed air. [b]Determined by GPC in trichlorobenzene at 150 °C. [c]Determined by high temperature NMR spectroscopy.

Ethylene Polymerization Studies. Once we established the speciation and structures of the nickel-alkali species in solution, we evaluated their reactivity with ethylene. Our reactions were performed by combining a nickel catalyst (1.0 equiv.), $MBAr^F_4$ (1.0 equiv., if any), and the activator $Ni(COD)_2$ (COD = 1,5-cyclooctadiene) in 50 mL of toluene/Et_2O (96:4) and then stirring at 25 °C under 200 psi of ethylene (Table 1). In the absence of alkali salts, **Ni1** (entry 1) and **Ni2** (entry 6) exhibited identical activity (2 kg/mol Ni·h) and gave polymers with similar molecular weight (~2 kg/mol) and branching (≤ 34/1000 C). These results were expected given that the nickel centers in **Ni1** and

Ni2 have similar structural and electronic environments. As control, reactions conducted without the nickel catalyst or $Ni(COD)_2$ did not yield any polymer products (Table S3).

In the presence of alkali salts, both nickel complexes displayed enhanced catalytic performance (Table 1). For example, the addition of Li^+ to **Ni2** (entry 7) increased activity by 166×, polymer molecular weight by 9×, and polymer branching by 3× relative to that observed using only **Ni2** (entry 6). Consistent with our previous studies,[25,26] the extent of change in these catalytic parameters are dependent on the cation used, demonstrating that our nickel catalysts are cation tunable. Most strikingly, polymerizations using **Ni2**+M^+ were more efficient relative to those using the corresponding **Ni1**+M^+. For example, the catalyst activity increased 72× (entry 7 vs. 2), 5× (entry 8 vs. 3), 4× (entry 9 vs. 4), and 1.5× (entry 10 vs. 5) for the Li^+, Na^+, K^+, and Cs^+ based reactions, respectively. We found that this trend also holds at different reaction times (0.5-2 h, Table S4), temperature (25-75 °C, Table S5), and ethylene pressures (100-400 psi, Table S6). It is notable that the cation effect is maintained at temperatures up to 75°C, giving higher catalyst activity, polymer MW, and polymer branching (Table S5) relative to that of the parent **Ni2** without cations. These results clearly demonstrate that the modified ligand of **Ni2** is a better supporting platform for generating highly active nickel-alkali species compared to the parent ligand of **Ni1**.

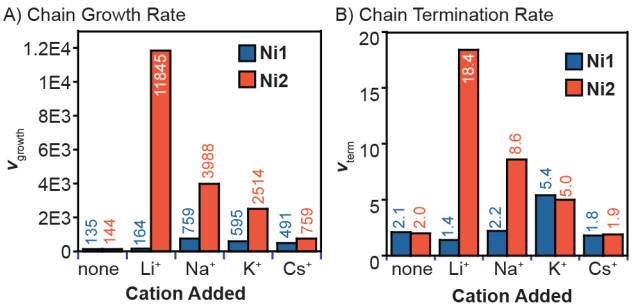

Figure 4. Comparison of the chain growth (A) and chain termination (B) rates observed for the various nickel and nickel-alkali catalysts in ethylene polymerization. Rate units: v_{growth} = mol C_2H_4/mol Ni·h; v_{term} = mol polyethylene/mol Ni·h.

To understand the cation effects on the polymerization process, we compared the rates of chain growth (v_{growth}, Figure S10) and chain termination (v_{term}, Figure S11) derived from the polymerization data. We observed that in all cases, v_{growth} was larger for **Ni2**-M than **Ni1**-M (Figure 4A). The rates for **Ni2**-M follow the periodic trend $Li^+ > Na^+ > K^+ > Cs^+$ whereas the rates for **Ni1**-M do not. It has been shown that electron-poor catalysts tend to undergo chain propagation faster than their electron-rich counterparts due to having lower ethylene insertion barriers.[48] Because the alkali ions are closer to the nickel centers in **Ni2**-M than in **Ni1**-M, the catalytic sites in the former likely experience greater electrostatic charge and electron induction.

In terms of chain termination, only **Ni2**-Li and **Ni2**-Na exhibited higher v_{term} than that of the corresponding **Ni1**-Li and **Ni1**-Na, respectively (Figure 4B). Given that electron-poor catalysts favor β-hydride elimination[49] but bulky catalysts disfavor polymer chain displacement,[50,51] competing effects may be operative. We propose that although **Ni2**-M is more electron-poor compared to **Ni1**-M, which increases v_{term}, the greater rigidity of its 2,6-diisopropylphenyl group decreases v_{term} by shielding the nickel axial sites more effectively. Based on the v_{growth}/v_{term} ratios, it appears that the significantly enhanced chain growth relative to chain termination rates in **Ni2**-M are responsible for its higher polymer molecular weight and lower branching density compared to that in **Ni1**-M.

CONCLUSIONS

We have developed a second-generation nickel phenoxyimine catalyst **Ni2** that forms stable adducts with alkali ions and exhibits cation tunable reactivity. Unlike the first-generation catalyst, **Ni2** bears a PEG moiety that is attached to the phenolate ring via a methylene unit. This seemingly minor change led to significant improvements in its properties, including the ability to form 1:1 nickel:alkali species in solution and the positioning of the pendant cation closer to the active site. Our studies suggest that these factors may be responsible for the superior performance of **Ni2**-M relative to that of **Ni1**-M in ethylene polymerization, giving higher catalyst activity and higher polymer molecular weight. Presumably, the closer proximity of the alkali ion to nickel in **Ni2**-M increases the electrostatic charge and electron induction experienced by the Ni center. However, further studies are needed to quantify the contributions of the various effects. This work has provided a better understanding of the design criteria for creating cation-responsive olefin polymerization catalysts. In particular, to achieve maximum cation effects, the binding pocket must enable formation of discrete 1:1 nickel:alkali species and the resulting adduct must adopt a conformation that allows effective steric shielding and electronic communication with the active site.

EXPERIMENTAL SECTION

General Procedures. Commercial reagents were used as received. The Li^+, Na^+, K^+, and Cs^+ $BAr^F{}_4^-$ salts were synthesized according to literature procedures.[52,53] Compounds **2** and **Ni1** were prepared as described previously.[41] All air and moisture sensitive manipulations were performed using standard Schlenk techniques or under a nitrogen atmosphere using a glovebox. Anhydrous solvents were obtained from an Innovative Technology solvent drying system saturated with argon. High-resolution mass spectra were obtained from the mass spectral facility at the University of Texas at Austin. IR data were obtained using a ThermoNicolet Avator 360 FT-IR instrument. NMR spectra were acquired using JEOL spectrometers (ECA-400, 500, and 600) and referenced using residual solvent peaks. All ^{13}C NMR spectra were proton decoupled. ^{31}P NMR spectra were referenced to phosphoric acid. For polymer characterization, ^1H NMR spectroscopy: each NMR sample contained ~15 mg of polymer in 0.6 mL of 1,1,2,2-tetrachloroethane-d_2 (TCE-d_2) and was recorded on a 600 MHz spectrometer using standard acquisition parameters at 120 °C. ^{13}C NMR spectroscopy: each NMR sample contained ~50 mg of polymer in 0.6 mL of TCE-d_2 and was recorded at 120 °C (151 MHz). The samples were acquired using a 90° pulse of 11.7 μs, a relaxation delay of 4 s, an acquisition time of 0.81 s, and inverse gated decoupling. The samples were preheated for 20 min prior to data acquisition. The polymer ^{13}C NMR spectra were assigned based on the chemical shift values reported in the literature.[54] Gel permeation chromatography (GPC) data were obtained using a Malvern high temperature GPC instrument equipped with refractive index, viscometer, and light scattering detectors at 150 °C with 1,2,4-trichlorobenzene (stabilized with 125 ppm BHT) as the mobile phase. The GPC instrument was calibrated using narrow polystyrene standards with universal calibration. All polymer molecular weights reported are based on the triple detection method.

Synthesis and Characterization

Complex Ni2. Inside the glovebox, the deprotonated salt of **4** (70 mg, 0.14 mmol, 1.0 equiv.) and $NiBr(Ph)(PPh_3)_2$ (104 mg, 0.14 mmol, 1.0 equiv.) were combined in 15 mL of THF. The mixture was stirred at room temperature for 4 h. The resulting red solution was filtered through celite in a pipet plug and then dried under vacuum to give a dark red oil. The crude material was dried and recrystallized in THF and pentane to yield yellow crystals (0.11 g, 94%). ^{1}H NMR (benzene-d_6, 400 MHz): δ 1.09 (d, 6H), 1.11 (d, 6H), 2.14 (s, 3H), 3.12 (s, 3H), 3.30 (m, 4H), 3.47 (m, 8H), 3.70 (s, 2H), 4.1 (m, 2H), 6.31 (m, 3H), 6.75 (s, 1H), 6.86-6.94 (m, 9H), 6.96-6.99 (m, 3H), 7.00-7.04 (m, 3H), 7.63 (m, 7H), 7.95 (d, 1H). ^{13}C NMR (benzene-d_6, 101 MHz): δ 20.60, 22.88 (s, 2C), 25.86 (s, 2C), 29.08 (s, 2C), 58.71, 68.20, 70.34, 70.75, 70.92, 71.08, 71.10, 72.39, 118.14, 121.54, 122.91 (s, 2C), 125.41, 126.19, 127.94, 128.17 (s, 2C), 128.50, 128.80, 128.87 (s, 2C), 129.93, 129.95, 131.59, 131.69, 131.84, 132.27, 133.59, 134.11 (s, 2C), 134.30, 134.64, 134.74 (s, 2C), 137.97, 138.00, 138.03, 138.09, 140.82 (s, 2C), 147.09, 147.58, 150.51, 161.68, 166.33. ^{31}P NMR (benzene-d_6, 162 MHz): δ 26.43 ppm. FT-IR: (ν_{CONi}), 1547(ν_{CN}) cm^{-1}. HRMS-ESI(+): Calc. for $C_{52}H_{60}NNiO_5P$ $[M+Na]^+$ = 890.3455, found = 890.3456.

Metal Binding Studies (UV-vis Absorption Spectroscopy). Stock solutions of **Ni1**, **Ni2**, and $MBAr^F_4$ (M = Li^+, Na^+, K^+, Cs^+) were prepared inside a nitrogen-filled glovebox. A 500 μM stock solution of Ni complexes was obtained by dissolving 25 μmol of a Ni complex in 50 mL of Et_2O. A 10 mL aliquot of this 500 μM solution was diluted to 50 mL using a volumetric flask to give a final concentration of 100 μM. The 3.0 mM stock solution of $MBAr^F_4$ was obtained by dissolving 30 μmol of $MBAr^F_4$ in 10 mL of Et_2O using a volumetric flask. A 3.0 mL solution of Ni complexes was transferred to a 1.0 cm quartz cuvette and then sealed with a septum screw cap. The cuvette was placed inside a UV-Vis spectrophotometer and the spectrum of the Ni solution was recorded. Aliquots containing 0.1 equiv. of $MBAr^F_4$ (10 μL), relative to the nickel complex, were added and the solution was allowed to reach equilibrium before the spectra were measured (15 min). The titration experiments were stopped after the addition of up to 1.0 equiv. of $MBAr^F_4$.

Metal Binding Studies (NMR Spectroscopy). The electronic effects of the secondary metals upon binding to **Ni2** and **Ni1** were studied via ^{1}H and ^{31}P NMR spectroscopy. To prepare each sample, 5 μmol of **Ni2** or **Ni1** and 7.5 μmol (1.5 equiv. relative to Ni) of $MBAr^F_4$ were dissolved in 5 mL of dry Et_2O and stirred for 30 min. The bright orange solution was evaporated to dryness to obtain an orange-red solid. This complex was dissolved in 0.6 mL of a stock solution of dry toluene-d_8/Et_2O (2:1 v/v), transferred to an NMR tube, and then analyzed by ^{1}H and ^{31}P NMR spectroscopy. NMR samples containing only $MBAr^F_4$ in the same solvent mixture were also analyzed as a control to measure the shift in the ^{1}H NMR peaks corresponding to the $BAr^F_4{}^-$ anion. Additionally, samples containing Ni and varying equiv. of $NaBAr^F_4$ (0.5 and 1.0 equiv. relative to Ni) were also tested to probe the differences in Ni and M^+ binding between different catalysts.

Computational Methods. Density functional theory (DFT) calculations were carried out using *Gaussian 16* Revision C.01.[55] Optimizations and frequency calculations were computed with the ωB97X-D functional and the def2-SVP basis set. Given the size of these complexes, this combination provided a balance of computational cost and insight. All calculations were carried out in the gas-phase. All stationary points were confirmed minima by the absence of any imaginary normal-mode frequencies (i.e., negative eigenvalues).

Polymerization Studies. Inside the glovebox, the nickel catalyst (24 μmol) and 1 equiv. of $MBAr^F_4$ (M = Li^+, Na^+, K^+, or Cs^+) were dissolved in 6 mL of toluene/diethyl ether (2:1 v:v) in a 20 mL vial and stirred for 10 min. Solid $Ni(COD)_2$ (2.0 equiv.) was added and stirred until a homogenous solution was obtained (~5 min). The mixture was loaded into a 10 mL gas-tight Hamilton syringe equipped with an 8-inch stainless steel needle. The loaded syringe was sealed by closing the syringe valve and a piece of rubber septum was attached to the tip of the needle to prevent exposure to air outside of the glovebox. To prepare the polymerization reactor, 44 mL of dry toluene was placed in an empty autoclave. The autoclave was pressurized with ethylene, and then the reactor pressure was reduced to 5 psi. This process was repeated 3 times to remove trace amounts of air inside the reaction vessel. The catalyst solution was then brought outside of the glovebox and then injected into the autoclave through a side arm. The reactor pressure was increased to the desired pressure, and the contents were stirred vigorously during polymerization. To stop the polymerization, the autoclave was vented and MeOH (200 mL) was added to precipitate the polymer and treated with 1 mL of concentrated HCl (37%). The polymer was collected by vacuum filtration, rinsed with MeOH, and dried under vacuum overnight. The reported yields are average values obtained from duplicate or triplicate runs.

ASSOCIATED CONTENT

Supporting Information

The Supporting Information is available free of charge on the ACS Publications website.

Synthesis procedures, titration data, NMR spectra, crystallographic data, DFT calculations (PDF)

Coordinates of eight DFT calculated structures combined in a single file (.xyz)

AUTHOR INFORMATION

Corresponding Author

Loi H. Do- Department of Chemistry, University of Houston, Houston, Texas 77004, United States;

Email: loido@uh.edu

Authors

Lorenzo C. Ruiz de Castilla- Department of Chemistry, University of Houston, Houston, Texas 77004, United States

Tuhin Ganguly- Department of Chemistry, University of Houston, Houston, Texas 77004, United States

Babak Tahmouresilerd- Department of Chemistry, University of Houston, Houston, Texas 77004, United States

Croix J. Laconsay- Department of Chemistry, University of Houston, Houston, Texas 77004, United States

Judy I. Wu- Department of Chemistry, University of Houston, Houston, Texas 77004, United States

ACKNOWLEDGMENT

We are grateful to the National Science Foundation (CHE-2154532 to L.H.D.), National Institute of General Medicine Sciences of the National Institutes of Health (R35GM133548 to J.I.W.), and the Alfred P. Sloan Research Foundation (FG-2020-12811 to J.I.W.) for support.

CONFLICTS OF INTEREST

The authors declare no competing financial interests.

REFERENCES

(1) Braunschweig, H.; Breitling, F. M. Constrained geometry complexes—Synthesis and applications. *Coord. Chem. Rev.*, **2006**, *250*, 2691-2720.

(2) Chum, P. S.; Swogger, K. W. Olefin polymer technologies—History and recent progress at The Dow Chemical Company. *Prog. Polym. Sci.*, **2008**, *33*, 797-819.

(3) Capacchione, C.; Grisi, F.; Lamberti, M.; Mazzeo, M.; Milani, B.; Milione, S.; Pappalardo, D.; Zuccaccia, C.; Pellecchia, C. Metal Catalyzed Polymerization: From Stereoregular Poly(α-olefins) to Tailor-Made Biodegradable/Biorenewable Polymers and Copolymers. *Eur. J. Inorg. Chem.*, **2023**, *26*, e202200644.

(4) Ittel, S. D.; Johnson, L. K.; Brookhart, M. Late-Metal Catalysts for Ethylene Homo- and Copolymerization. *Chem. Rev.*, **2000**, *100*, 1169-1203.

(5) Nakamura, A.; Ito, S.; Nozaki, K. Coordination-Insertion Copolymerization of Fundamental Polar Monomers. *Chem. Rev.*, **2009**, *109*, 5215-5244.

(6) Nakamura, A.; Anselment, T. M. J.; Claverie, J.; Goodall, B.; Jordan, R. F.; Mecking, S.; Rieger, B.; Sen, A.; van Leeuwen, P. W. N. M.; Nozaki, K. *Ortho*-Phosphinobenzenesulfonate: A Superb Ligand for Palladium-Catalyzed Coordination-Insertion Copolymerization of Polar Vinyl Monomers. *Acc. Chem. Res.*, **2013**, *46*, 1438-1449.

(7) Chen, Z.; Brookhart, M. Exploring Ethylene/Polar Vinyl Monomer Copolymerizations Using Ni and Pd α-Diimine Catalysts. *Acc. Chem. Res.*, **2018**, *51*, 1831-1839.

(8) Wu, R.; Wu, W. K.; Stieglitz, L.; Gaan, S.; Rieger, B.; Heuberger, M. Recent advances on α-diimine Ni and Pd complexes for catalyzed ethylene (Co)polymerization: A comprehensive review. *Coord. Chem. Rev.*, **2023**, *474*, 214844.

(9) Mu, H.; Zhou, G.; Hu, X.; Jian, Z. Recent advances in nickel mediated copolymerization of olefin with polar monomers. *Coord. Chem. Rev.*, **2021**, *435*, 213802.

(10) Xin, B. S.; Sato, N.; Tanna, A.; Oishi, Y.; Konishi, Y.; Shimizu, F. Nickel Catalyzed Copolymerization of Ethylene and Alkyl Acrylates. *J. Am. Chem. Soc.*, **2017**, *139*, 3611-3614.

(11) Johnson, L. K.; Killian, C. M.; Brookhart, M. New Pd(II)- and Ni(II)-Based Catalysts for Polymerization of Ethylene and α-Olefins. *J. Am. Chem. Soc.*, **1995**, *117*, 6414-6415.

(12) Svejda, S. A.; Johnson, L. K.; Brookhart, M. Low-Temperature Spectroscopic Observation of Chain Growth and Migratory Insertion Barriers in (α-Diimine)Ni(II) Olefin Polymerization Catalysts. *J. Am. Chem. Soc.*, **1999**, *121*, 10634-10635.

(13) Younkin, T. R.; Connor, E. F.; Henderson, J. I.; Friedrich, S. K.; Grubbs, R. H.; Bansleben, D. A. Neutral, Single-Component Nickel(II) Polyolefin Catalysts That Tolerate Heteroatoms. *Science*, **2000**, *287*, 460-462.

(14) Connor, E. F.; Younkin, T. R.; Henderson, J. I.; Waltman, A. W.; Grubbs, R. H. Synthesis of Neutral Nickel Catalysts for Ethylene Polymerization–The Influence of Ligand Size on Catalyst Stability. *Chem. Commun.*, **2003**, 2272-2273.

(15) Wang, X.; Xu, M.; Zhang, S.; Qasim, M.; Chen, M. Fluorine Effect on α-Imino-ketone- and Phenoxyiminato Nickel-Catalyzed Ethylene Homo- and Copolymerization. *Organometallics*, **2022**, *41*, 1078-1086.

(16) Liang, T.; Goudari, S. B.; Chen, C. A simple and versatile nickel platform for the generation of branched high molecular weight polyolefins. *Nat. Commun.*, **2020**, *11*, 372.

(17) Laine, T. V.; Lappalainen, K.; Liimatta, J.; Aitola, E.; Löfgren, B.; Leskelä, M. Polymerization of ethylene with new diimine complexes of late transition metals. *Macromol. Rapid Commun.*, **1999**, *20*, 487-491.

(18) Benito, J. M.; de Jesús, E.; de la Mata, F. J.; Flores, J. C.; Gómez, R.; Gómez-Sal, P. Mononuclear and Dendritic Nickel(II) Complexes Containing N,N′ -Iminopyridine Chelating Ligands: Generation Effects on the Catalytic Oligomerization and Polymerization of Ethylene. *Organometallics*, **2006**, *25*, 3876-3887.

(19) Medina, J. T.; Tran, Q. H.; Hughes, R. P.; Wang, X.; Brookhart, M.; Daugulis, O. Ethylene Polymerizations Catalyzed by Fluorinated "Sandwich" Diimine-Nickel and Palladium Complexes. *J Am Chem Soc*, **2024**, *146*, 15143-15154.

(20) Ji, G.; Chen, Z.; Wang, X.-Y.; Ning, X.-S.; Xu, C.-J.; Zhang, X.-M.; Tao, W.-J.; Li, J.-F.; Gao, Y.; Shen, Q.; Sun, X.-L.; Wang, H.-Y.; Zhao, J.-B.; Zhang, B.; Guo, Y.-L.; Zhao, Y.; Sun, J.; Luo, Y.; Tang, Y. Direct copolymerization of ethylene with protic comonomers enabled by multinuclear Ni catalysts. *Nat. Commun.*, **2021**, *12*, 6283.

(21) Teator, A. J.; Lastovickova, D. N.; Bielawski, C. W. Switchable Polymerization Catalysts. *Chem. Rev.*, **2016**, *116*, 1969-1992.

(22) Tran, T. V.; Do, L. H. Tunable Modalities in Polyolefin Synthesis via Coordination Insertion Catalysis. *Eur. Polym. J.*, **2021**, *142*, 110100.

(23) Doerr, A. M.; Burroughs, J. M.; Gitter, S. R.; Yang, X.; Boydston, A. J.; Long, B. K. Advances in Polymerizations Modulated by External Stimuli. *ACS Catal.*, **2020**, *10*, 14457-14515.

(24) Johnson, L.; Wang, L.; McLain, S.; Bennett, A.; Dobbs, K.; Hauptman, E.; Ionkin, A.; Ittel, S.; Kunitsky, K.; Marshall, W.; McCord, E.; Radzewich, C.; Rinehart, A.; Sweetman, K. J.; Wang, Y.; Yin, Z.; Brookhart, M. Copolymerization of Ethylene and Acrylates by Nickel Catalysts. In *Beyond Metallocenes*; American Chemical Society: 2003; Vol. 857, p 131-142.

(25) Cai, Z.; Xiao, D.; Do, L. H. Fine-Tuning Nickel Phenoxyimine Olefin Polymerization Catalysts: Performance Boosting by Alkali Cations. *J. Am. Chem. Soc.*, **2015**, *137*, 15501-15510.

(26) Cai, Z.; Do, L. H. Customizing Polyolefin Morphology by Selective Pairing of Alkali Ions with Nickel Phenoxyimine-Polyethylene Glycol Catalysts. *Organometallics*, **2017**, *36*, 4691-4698.

(27) Tran, T. V.; Lee, E.; Nguyen, Y. H.; Nguyen, H. D.; Do, L. H. Customizing Polymers by Controlling Cation Switching Dynamics in Non-Living Polymerization. *J. Am. Chem. Soc.*, **2022**, *144*, 17129-17139.

(28) Smith, A. J.; Kalkman, E. D.; Gilbert, Z. W.; Tonks, I. A. $ZnCl_2$ Capture Promotes Ethylene Polymerization by a Salicylaldiminato Ni Complex Bearing a Pendent 2,2′ -Bipyridine Group. *Organometallics*, **2016**, *35*, 2429-2432.

(29) Akita, S.; Nozaki, K. Copolymerization of Ethylene and Methyl Acrylate by Palladium Catalysts Bearing IzQO Ligands Containing Methoxyethyl Ether Moieties and Salt Effects for Polymerization. *Polym. J.*, **2021**, *53*, 1057–1060.

(30) Xiong, S.; Spinney, H. A.; Bailey, B. C.; Henderson, B. S.; Tekpor, A. A.; Espinosa, M. R.; Saha, P.; Agapie, T. Switchable Synthesis of Ethylene/Acrylate Copolymers by a Dinickel Catalyst: Evidence for Chain Growth on Both Nickel Centers and Concepts of Cation Exchange Polymerization. *ACS Catal.*, **2024**, *14*, 5260-5268.
(31) Chiu, H.-C.; Koley, A.; Dunn, P. L.; Hue, R. J.; Tonks, I. A. Ethylene polymerization catalyzed by bridging Ni/Zn heterobimetallics. *Dalton Trans.*, **2017**, *46*, 5513-5517.
(32) Xiong, S.; Shoshani, M. M.; Nett, A. J.; Spinney, H. A.; Henderson, B. S.; Agapie, T. Nickel-Based Heterometallic Catalysts for Ethylene-Acrylate Copolymerization: Interrogating Effects of Secondary Metal Additives. *Organometallics*, **2023**, *42*, 2849-2855.
(33) Chiu, H.-C.; Pearce, A. J.; Dunn, P. L.; Cramer, C. J.; Tonks, I. A. β-Oxo-δ-diimine Nickel Complexes: A Comparison of Tautomeric Active Species in Ethylene Polymerization Catalysis. *Organometallics*, **2016**, *35*, 2076-2085.
(34) Zhang, Y.; Mu, H.; Pan, L.; Wang, X.; Li, Y. Robust Bulky [P,O] Neutral Nickel Catalysts for Copolymerization of Ethylene with Polar Vinyl Monomers. *ACS Catal.*, **2018**, *8*, 5963-5976.
(35) Zhang, Y.; Mu, H.; Wang, X.; Pan, L.; Li, Y. Elaborate Tuning in Ligand Makes a Big Difference in Catalytic Performance: Bulky Nickel Catalysts for (Co)polymerization of Ethylene with Promising Vinyl Polar Monomers. *ChemCatChem*, **2019**, *11*, 2329-2340.
(36) Zhang, Y.; Wang, F.; Pan, L.; Wang, B.; Li, Y. Facile Synthesis of High-Molecular-Weight Vinyl Sulfone (Sulfoxide) Modified Polyethylenes via Coordination–Insertion Copolymerization. *Macromolecules*, **2020**, *53*, 5177-5187.
(37) Wang, X.-l.; Zhang, Y.-p.; Wang, F.; Pan, L.; Wang, B.; Li, Y.-s. Robust and Reactive Neutral Nickel Catalysts for Ethylene Polymerization and Copolymerization with a Challenging 1,1-Disubstituted Difunctional Polar Monomer. *ACS Catal.*, **2021**, *11*, 2902-2911.
(38) Berkefeld, A.; Drexler, M.; Möller, H. M.; Mecking, S. Mechanistic Insights on the Copolymerization of Polar Vinyl Monomers with Neutral Ni(II) Catalysts. *J. Am. Chem. Soc.*, **2009**, *131*, 12613-12622.
(39) Waltman, A. W.; Younkin, T. R.; Grubbs, R. H. Insights into the Deactivation of Neutral Nickel Ethylene Polymerization Catalysts in the Presence of Functionalized Olefins. *Organometallics*, **2004**, *23*, 5121-5123.
(40) Tahmouresilerd, B.; Xiao, D.; Do, L. H. Rigidifying Cation-Tunable Nickel Catalysts Increases Activity and Polar Monomer Incorporation in Ethylene and Methyl Acrylate Copolymerization. *Inorg. Chem.*, **2021**, *60*, 19035-19043.
(41) Tran, T. V.; Nguyen, Y. H.; Do, L. H. Development of Highly Productive Nickel–Sodium Phenoxyphosphine Ethylene Polymerization Catalysts and their Reaction Temperature Profiles. *Polym. Chem.*, **2019**, *10*, 3718-3721.
(42) Tran, T. V.; Karas, L. J.; Wu, J. I.; Do, L. H. Elucidating Secondary Metal Cation Effects on Nickel Olefin Polymerization Catalysts. *ACS Catal.*, **2020**, *10*, 10760-10772.
(43) Hibbert, D. B.; Thordarson, P. The death of the Job plot, transparency, open science and online tools, uncertainty estimation methods and other developments in supramolecular chemistry data analysis. *Chem. Commun.*, **2016**, *52*, 12792-12805.
(44) Thordarson, P. Determining association constants from titration experiments in supramolecular chemistry. *Chem. Soc. Rev.*, **2011**, *40*, 1305-1323.
(45) Tong, J.; Liu, S.; Zhang, S.; Li, S. Z. Prediction of ^{31}P nuclear magnetic resonance chemical shifts for phosphines. *Spectrochim. Acta A*, **2007**, *67*, 837-846.
(46) Payard, P.-A.; Perego, L. A.; Grimaud, L.; Ciofini, I. A DFT Protocol for the Prediction of ^{31}P NMR Chemical Shifts of Phosphine Ligands in First-Row Transition-Metal Complexes. *Organometallics*, **2020**, *39*, 3121-3130.
(47) Apilardmongkol, P.; Ratanasak, M.; Hasegawa, J.-y.; Parasuk, V. Exploring the Reaction Mechanism of Heterobimetallic Nickel-Alkali Catalysts for Ethylene Polymerization: Secondary-Metal-Ligand Cooperative Catalysis. *ChemCatChem*, **2022**, *14*, e202200028.
(48) Malinoski, J. M.; Brookhart, M. Polymerization and Oligomerization of Ethylene by Cationic Nickel(II) and Palladium(II) Complexes Containing Bidentate Phenacyldiarylphosphine Ligands. *Organometallics*, **2003**, *22*, 5324-5335.
(49) Heinicke, J.; Köhler, M.; Peulecke, N.; He, M.; Kindermann, M. K.; Keim, W.; Fink, G. 2-Phosphanylphenolate Nickel Catalysts for the Polymerization of Ethylene. *Chem.- Eur. J.*, **2003**, *9*, 6093-6107.
(50) Zhang, D.; Nadres, E. T.; Brookhart, M.; Daugulis, O. Synthesis of Highly Branched Polyethylene Using "Sandwich" (8-*p*-Tolyl naphthyl α-diimine)nickel(II) Catalysts. *Organometallics*, **2013**, *32*, 5136-5143.
(51) Camacho, D. H.; Salo, E. V.; Ziller, J. W.; Guan, Z. Cyclophane-Based Highly Active Late-Transition-Metal Catalysts for Ethylene Polymerization. *Angew. Chem. Int. Ed.*, **2004**, *43*, 1821-1825.
(52) Brookhart, M.; Grant, B.; Volpe, A. F., Jr. [(3,5-$(CF_3)_2C_6H_3)_4$B]-[$H(OEt_2)_2$]$^+$: A Convenient Reagent for Generation and Stabilization of Cationic, Highly Electrophilic Organometallic Complexes. *Organometallics*, **1992**, *11*, 3920-3922.
(53) Carreras, L.; Rovira, L.; Vaquero, M.; Mon, I.; Martin, E.; Benet-Buchholz, J.; Vidal-Ferran, A. Syntheses, characterisation and solid-state study of alkali and ammonium BArF salts. *RSC Adv.*, **2017**, *7*, 32833-32841.
(54) Galland, G. B.; de Souza, R. F.; Mauler, R. S.; Nunes, F. F. ^{13}C NMR Determination of the Composition of Linear Low-Density Polyethylene Obtained with [η^3-Methallyl-Nickel-Diimine]PF_6 Complex. *Macromolecules*, **1999**, *32*, 1620-1625.
(55) Frisch, M. J.; Trucks, G. W.; Schlegel, H. B.; Scuseria, G. E.; Robb, M. A.; Cheeseman, J. R.; Scalmani, G.; Barone, V.; Petersson, G. A.; Nakatsuji, H.; Li, X.; Caricato, M.; Marenich, A. V.; Bloino, J.; Janesko, B. G.; Gomperts, R.; Mennucci, B.; Hratchian, H. P.; Ortiz, J. V.; Izmaylov, A. F.; Sonnenberg, J. L.; Williams; Ding, F.; Lipparini, F.; Egidi, F.; Goings, J.; Peng, B.; Petrone, A.; Henderson, T.; Ranasinghe, D.; Zakrzewski, V. G.; Gao, J.; Rega, N.; Zheng, G.; Liang, W.; Hada, M.; Ehara, M.; Toyota, K.; Fukuda, R.; Hasegawa, J.; Ishida, M.; Nakajima, T.; Honda, Y.; Kitao, O.; Nakai, H.; Vreven, T.; Throssell, K.; Montgomery Jr., J. A.; Peralta, J. E.; Ogliaro, F.; Bearpark, M. J.; Heyd, J. J.; Brothers, E. N.; Kudin, K. N.; Staroverov, V. N.; Keith, T. A.; Kobayashi, R.; Normand, J.; Raghavachari, K.; Rendell, A. P.; Burant, J. C.; Iyengar, S. S.; Tomasi, J.; Cossi, M.; Millam, J. M.; Klene, M.; Adamo, C.; Cammi, R.; Ochterski, J. W.; Martin, R. L.; Morokuma, K.; Farkas, O.; Foresman, J. B.; Fox, D. J. *Gaussian 16 Rev. C.01*; Gaussian 16: Wallingford, CT, 2016.

Table of Contents